AGU100 ADVANCING EARTH AND SPACE SCIENCE

Geophysical Research Letters

RESEARCH LETTER
10.1029/2018GL078752

Simulating Short-Term Evolution of Slow Slip Influenced by Fault Heterogeneities and Tides

Yajun Peng[1] **and Allan M. Rubin**[1]

[1]Department of Geosciences, Princeton University, Princeton, NJ, USA

Key Points:
- In multiple subduction zones, tremor during slow slip events occurs in short, repetitive bursts with increasing recurrence intervals
- We reproduce this behavior numerically by assuming that the repetitive bursts are driven by surrounding, steadier slow slip
- With external sinusoidal loading added to mimic tides, recurrence intervals increase until coinciding approximately with the loading period

Supporting Information:
- Supporting Information S1
- Data Set S1
- Data Set S2

Correspondence to:
Y. Peng,
yajun@alumni.princeton.edu

Citation:
Peng, Y., & Rubin, A. M. (2018). Simulating short-term evolution of slow slip influenced by fault heterogeneities and tides. *Geophysical Research Letters*, *45*, 10,269–10,278. https://doi.org/10.1029/2018GL078752

Received 14 MAY 2018
Accepted 31 AUG 2018
Accepted article online 6 SEP 2018
Published online 2 OCT 2018

Abstract In this study, we analyze high-resolution tremor catalogs from northern Cascadia, Guerrero, and northern Kii Peninsula. We find that tremor often occurs in short bursts that repeatedly occupy the same source area within a slow slip event. We hypothesize that these bursts are driven by loading from slow slip in areas surrounding the tremor zone. Adopting a rate-and-state friction law with a velocity-weakening to velocity-strengthening transition, we develop a finite fault model in which the size of the slow slip zone is larger than that of the tremor zone. Tidal forcing is added. Many asperities are randomly distributed within the tremor zone in order to generate burst-like slip evolution while maintaining reasonable propagation speeds of the main slow slip front. We successfully reproduce the increasing recurrence intervals of the bursts as the main front moves across the tremor zone, as well as tidally modulated secondary fronts well behind the main front.

Plain Language Summary Episodic slow slip events, often accompanied by tectonic tremor, represent a significant component of the complete seismic cycle. However, their physical mechanisms remain elusive. In this study, we find that tremor in multiple subduction zones tends to occur in the form of short bursts. During a slow slip event, the tremor bursts, viewed as a proxy for the contemporaneous slow slip, occur repeatedly over the same source areas with recurrence intervals increasing until coinciding approximately with the tidal period. We successfully simulate this behavior with a laboratory-derived friction law. Our numerical model highlights the important role of fault heterogeneities and tides in controlling the short-term evolution of slow slip.

1. Introduction

Slow earthquake phenomena, including slow slip events (SSEs) and tectonic tremor, have been reported in many subduction zones (Beroza & Ide, 2011; Schwartz & Rokosky, 2007). SSEs possess several properties that are in distinct contrast to regular earthquakes, such as low average slip speeds (roughly one to two orders of magnitude above the plate rate) and slow main-front propagation speeds (of order 10^0–10^1 km/day; e.g., Houston et al., 2011; Obara, 2010). Previous studies have proposed several mechanisms to explain these properties, including standard rate-and-state friction on a fault near neutral stability (e.g., Liu & Rice, 2005, 2007), dilatant strengthening of fault gouge (e.g., Liu & Rubin, 2010; Segall et al., 2010; Suzuki & Yamashita, 2009), and a friction law that transitions from being steady-state velocity-weakening at low slip rate to steady-state velocity-strengthening at high slip rate (e.g., Hawthorne & Rubin, 2013b; Shibazaki & Iio, 2003; Shibazaki & Shimamoto, 2007). These studies typically assume a slow slip zone with homogeneous properties.

It has been widely documented that at least some portions of SSE source regions are capable of radiating weak seismic waves, that is, tectonic tremor (Beroza & Ide, 2011; Obara, 2002; Schwartz & Rokosky, 2007). In Cascadia and Japan, tremor and slow slip show significant spatial and temporal correlation (e.g., Hawthorne & Rubin, 2013a; Hirose & Obara, 2005, 2006; Obara & Hirose, 2006; Obara et al., 2004; Rogers & Dragert, 2003; Shelly et al., 2007; Wech et al., 2009). Bartlow et al. (2011) found that tremor locations closely tracked the areas of high slip rate during an SSE beneath southern Cascadia. Therefore, tremor has been generally thought to be a proxy for the contemporaneous slow slip. Previous studies have identified many tremor migrations with propagation speeds of order 10^2–10^3 km/day, one to two orders of magnitude faster than the main slow slip/tremor front (e.g., Bletery et al., 2017; Ghosh et al., 2010; Houston et al., 2011; Shelly et al., 2007). Some of the large-scale migrations are associated with significant moment-rate increases (Hawthorne et al., 2016). A possible explanation for the implied slip complexity is that the fault is heterogeneous. One proposal is that

tremor emanates from brittle patches embedded in a ductile matrix, which appears to be consistent with field observations of exhumed subduction fault zones (e.g., Fagereng et al., 2014). Conceivably, slow slip source regions with no observable tremor may be relatively homogeneous or may host patches of brittle material that are too small to accelerate to seismic slip speeds. A few previous studies (Ando et al., 2010; Luo & Ampuero, 2014; Skarbek et al., 2012) explored heterogeneous models for slow slip and tremor. High-resolution tremor observations can provide further constraints on this type of model.

Both slow slip and tremor appear to be sensitive to tidal modulation (e.g., Hawthorne & Rubin, 2010; Houston, 2015; Ide, 2010; Royer et al., 2014; Shelly et al., 2007), possibly resulting from high fluid pressure (low effective normal stress) in the source area (e.g., Audet & Kim, 2016; Shelly et al., 2006). In northern Cascadia, tidally modulated tremor bursts appear to most often occur as rapid tremor reversals (RTRs), secondary fronts that propagate tens of kilometers in the opposite direction of the main front (Houston et al., 2011; Peng & Rubin, 2016; Peng et al., 2015; Thomas et al., 2013). These RTRs propagate at speeds about 25 times faster than the main slow slip/tremor front (Houston et al., 2011). In this study, we summarize several key observations from high-resolution tremor catalogs beneath southern Vancouver Island, Canada (three major episodes from 2003 to 2005; Peng et al., 2015); the Olympic Peninsula, United States (two major episodes from 2010 to 2011; Peng & Rubin, 2016); Guerrero, Mexico (multiple episodes from 2005 to 2006; Peng & Rubin, 2017); and the northern Kii Peninsula, Japan (multiple episodes from 2004 to 2011; see supporting information S1). In section 3, we explore the effect of fault heterogeneity and tides on slow slip through numerical simulations.

2. Short-Term Slow Slip Evolution Revealed by High-Resolution Tremor Catalogs

Here we infer the slip evolution during SSEs from high-resolution tremor catalogs. We obtain these catalogs using cross-station cross correlations (Armbruster et al., 2014; Rubin & Armbruster, 2013). This method typically takes advantage of *S* wave coherence across different seismic stations that are separated by up to 30 km. The time offsets between stations are searched for by rotating the horizontal components of the seismograms at each station into the *S* wave polarization direction and then time shifting the stations to maximize the correlation. To improve the waveform similarity between the different stations, we corrected for shear-waves splitting for stations on southern Vancouver Island and stacked the aligned seismograms at individual small-aperture (1–2 km) arrays on the Olympic Peninsula (see Peng & Rubin, 2016, and Peng et al., 2015, for details). Although using a single trio of closely spaced stations generally limits the study area to be 30–70 km across, the cross-station method is capable of imaging fine patterns of tremor and reveals numerous migrations that last minutes to hours and propagate from two to tens of kilometers (Peng & Rubin, 2016, 2017; Peng et al., 2015; Rubin & Armbruster, 2013).

In Figures 1 and S1, we show the cross-station tremor catalogs during several representative SSEs in the four different regions. Beneath Cascadia and Japan, the main slow slip/tremor front can propagate up to a few hundred kilometers along strike during an episode (e.g., Houston et al., 2011; Obara, 2010; Wech et al., 2009). Beneath Guerrero, Radiguet et al. (2011) reported that a long-term SSE, which recurs every 3–4 years, showed slow along-strike propagation of the main front (~0.8 km/day). But the short-term SSEs, imaged by tremor locations near the downdip edge of the long-term SSEs, do not show such long-distance propagation (e.g., Frank et al., 2015; Peng & Rubin, 2017). Although generally less obvious, evidence for local main front propagation at speeds of 20 km/day can sometimes be identified in the short-term SSEs (Figure 1a of Peng & Rubin, 2017, and Figure 1g).

A common feature seen in these catalogs is that tremor tends to occur in short bursts that repeatedly occupy the same source area. This behavior is most conspicuous in areas with high tremor density and amplitude. To further illustrate this, we show the cumulative number of detections within a square region 3 km across (Figures 1b, 1e, 1h, and 1k). It appears that the tremor occurrence rate is high initially, indicating the arrival of the main slow slip/tremor front, and decreases with time. Since we do not have moment estimates for tremor, we treat the cumulative event number as a roughly proxy for slip accumulation. We find that as opposed to a smoothly increasing slip profile expected on a homogeneous fault, tremor occurs in an intermittent fashion. The recurrence intervals gradually increase with time, and eventually approach 12 and 24 hr, close to tidal periods. This can also be seen in the evolution of interdetection times (Figures 1c, 1f, 1i, and 1l). Sweet et al. (2012), Rubin and Armbruster (2013), and Bostock et al. (2015) also reported the same phenomenon in Cascadia, and it is consistent with the increased tidal sensitivity of tremor observed after several days of slip in northern Cascadia (Houston, 2015).

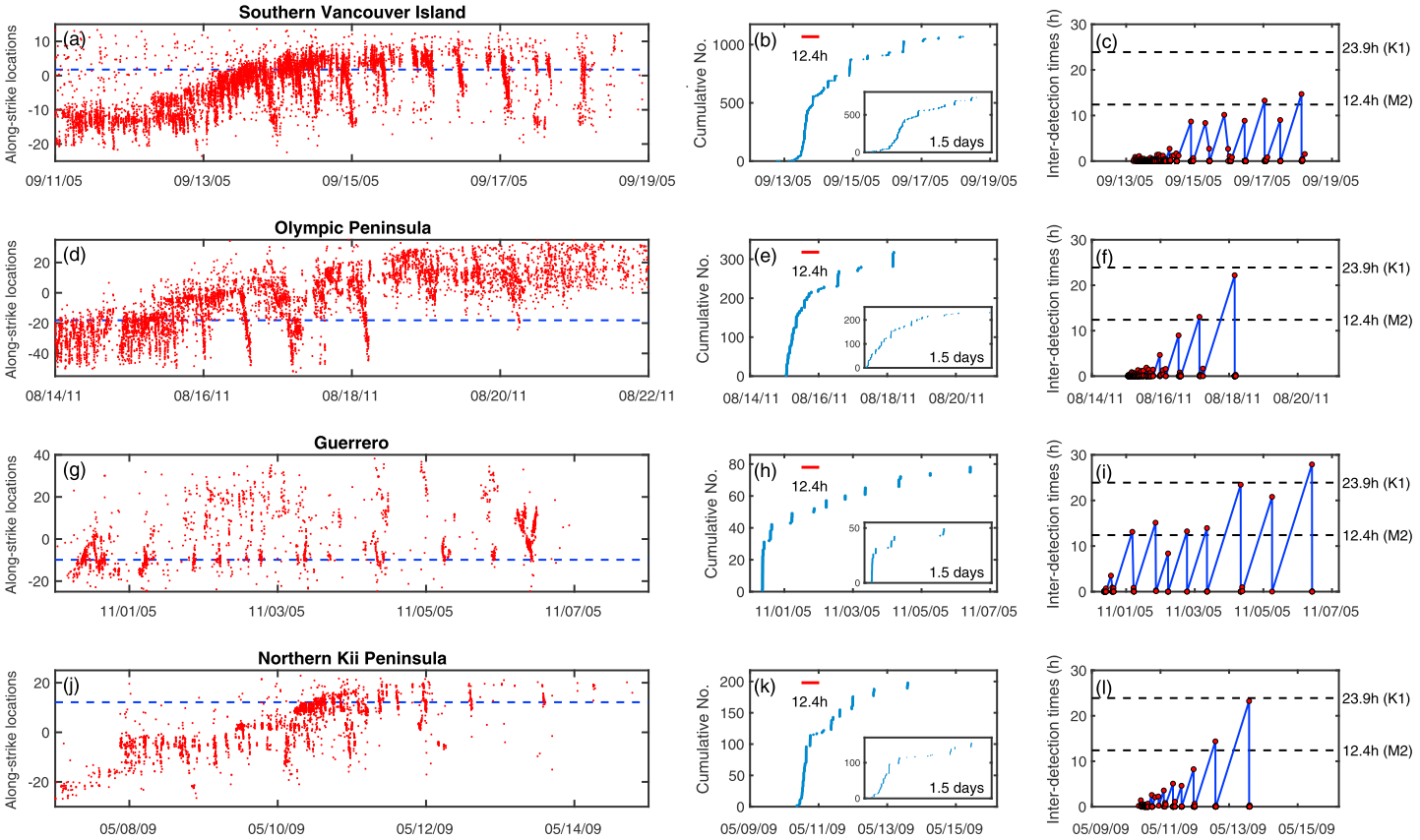

Figure 1. High-resolution tremor catalogs from southern Vancouver Island, Olympic Peninsula, Guerrero, and northern Kii Peninsula. The first column (a, d, g, and j) shows the along-strike tremor locations as a function of time during the slow slip event in each region. The blue-dashed line indicates the along-strike location of the square region 3 km across, within which the cumulative number of tremor detections over 7 days (the second column; b, e, h, and k) and the interdetection times (the third column, red circles; c, f, i, and l) are shown. The inset figures in the second column shows the cumulative number of detections during the first 1.5 days. The black-dashed lines in the third column show two tidal periods K1 (23.9 hr) and M2 (12.4 hr). See Figure S1 of the supporting information for additional examples.

One interpretation is that these bursts reflect tremor sources that are repeatedly driven to failure by surrounding slow slip (Peng & Rubin, 2016, 2017; Shelly et al., 2007). This would naturally explain the systematic increase in recurrence intervals, since the loading rate from the surrounding slip decreases as the front propagates away. In this scenario, the tidal stress does not provide the stress drop for these repetitive bursts but plays an important role in controlling their timing. This conceptual model implies that the slow slip zone in these regions should be larger than the tremor zone that hosts repetitive bursts (we refer to the latter as the tremor zone hereafter for simplicity). Furthermore, we expect that during an SSE, the total slip inside and outside the tremor zone is roughly the same. The intermittent nature of tremor suggests less time for slip, hence higher average slip rate, during the bursts within the tremor zone. In the following sections, we explore this conceptual model with numerical simulations.

3. Numerical Simulations

3.1. Friction Law

To simulate SSEs, we use a rate-and-state friction law with a velocity-weakening to velocity-strengthening transition (e.g., Dieterich, 2007):

$$\tau(V,\theta) = f^*\sigma + a\sigma \log\left(\frac{V}{V^*}\right) + b\sigma \log\left(\frac{V_c\theta}{D_c} + 1\right). \quad (1)$$

Here the frictional strength τ on the fault depends upon the slip rate V and the state θ. σ is the effective normal stress. V_c is the cutoff velocity for state evolution; for $\theta \ll D_c/V_c$, decreases in state no longer lead to decreases in strength. D_c represents a characteristic slip distance for state evolution, and a and b are nondimensional

constants that determine the dependence of frictional strength on slip rate and state. f^* and V^* are reference values of the friction coefficient and sliding velocity.

For state evolution with time, we choose the *aging* law:

$$\frac{d\theta}{dt} = 1 - \frac{V\theta}{D_c}. \tag{2}$$

The aging law was designed to model the time-dependent healing at zero slip rate (Beeler et al., 1994; Dieterich & Kilgore, 1994). The other commonly adopted formulation, the *slip* law, is better supported by laboratory experiments (Bhattacharya et al., 2015, 2017). But the aging law generally requires less resolution and hence makes our 2-D finite fault simulations more feasible. At steady state ($d\theta/dt = 0$), equation (2) implies $\theta = D_c/V$. Substituting this into equation (1) shows that there is a minimum steady state stress at the slip speed $V_{\tau_{min}} = \frac{b-a}{a}V_c$. For $V < V_{\tau_{min}}$, the steady state stress decreases with increasing slip rate, and for $V > V_{\tau_{min}}$, it increases (Figure S3).

Applying a linear stability analysis to equations (1) and (2), we obtain the critical spring stiffness for a spring-block-slider sliding at steady state at the load-point velocity V_{load} (see the supporting information S1):

$$k_{crit} = \frac{\sigma}{D_c}\left(\frac{b}{1 + V_{load}/V_c} - a\right). \tag{3}$$

Note that this k_{crit} is the same for both the aging law and the slip law, since the two are asymptotically the same near steady state. For $V_{load} \ll V_c$, k_{crit} converges to that of standard velocity weakening rate-and-state friction (Ruina, 1983). If we imagine that the loading comes from slow slip in the areas surrounding the tremor zone, then V_{load} evolves with time and could be very high (implying low k_{crit}) initially. We numerically simulate a spring-block-slider system with the spring stiffness k. By equating this k to k_{crit}, we obtain a critical loading rate V_{crit}, below which the block undergoes periodic slip oscillations:

$$V_{crit} = V_c\left(\frac{b\sigma}{kD_c + a\sigma} - 1\right). \tag{4}$$

Within this regime, the maximum slip rate increases with decreasing V_{load} (Figure S2); qualitatively, this result can be rationalized by noting that the available stress drop is tied to the difference between the steady-state stress at V_{load} and the minimum steady-state stress (Figure S3). For $V_{load} > V_{crit}$, sliding is stable. Equation (3) suggests that in order to simulate bursts that repeatedly occupy the same area, V_c (roughly the speed limit) within the tremor zone should be sufficiently large compared to the surrounding V_{load}.

3.2. Finite Fault Simulations

3.2.1. Model Setup

Here we adopt a simplified model geometry with a 2-D fault plane embedded in a 3-D homogeneous elastic medium. Fault slip is driven by the relative displacement, at rate V_0, of two rigid walls that are $W/2$ above and below the fault (Dublanchet et al., 2013; Horowitz & Ruina, 1989; Rice & Ruina, 1983). Elastic displacements are limited primarily by the distance to the slow slip front when that distance is less than $W/2$ and by the distance to the rigid walls when the distance to the slow slip front is greater than $W/2$. In this sense the separation W between the rigid walls roughly corresponds to the downdip extent of the slow slip zone in nature. Since we solve the elasticity equations in the wavenumber domain (see supporting information S1), the fault repeats indefinitely in both the *along-strike* and *along-dip* directions. The length of the fault along strike should be great enough that the slow slip front can propagate at least a few times W without being influenced by the along-strike repeats. We set the along-strike dimension of the fault to be $3W$. The slipping region is intentionally influenced by the along-dip repeats; this allows us to be faithful to the relevant constraints of elasticity while modeling a 2-D region narrower than W in the dip direction, which significantly reduces the computational expense compared to a model that includes the entire fault. We set W to be $500L_b$, where $L_b = \mu D_c/b\sigma$ is the characteristic length scale of the slip-weakening region at the rupture front, with μ being the elastic shear modulus (Rubin & Ampuero, 2005). The nucleation length scale $2L_\infty$ on a strictly velocity-weakening fault is $\frac{2}{\pi}(\frac{b}{b-a})^2 L_b$ (Rubin & Ampuero, 2005), about $16L_b$ given a^{bg} and b^{bg} in Table 1. For comparison, the fault width along dip is $150L_b$ ($0.3W$). In this model, SSEs spontaneously occur on the fault. Following Hawthorne and Rubin (2013b), we add a velocity-strengthening region to the fault with width of $0.15W$ in the along-strike

Table 1
List of Parameters Used

Parameters	Values
a^{bg} (background a)	0.008
b^{bg} (background b)	0.01
V_c^{bg} (background cutoff velocity)	5×10^{-8} m/s
a^{asp} (asperity a)	0.008
b^{asp} (asperity b)	0.01 (0.01 – 0.012 in supporting information S1)
V_c^{asp} (asperity cutoff velocity)	5×10^{-6} m/s (10^{-7} – 5×10^{-6} m/s in supporting information S1)
D_c (state evolution distance)	5×10^{-5} m
σ (effective normal stress)	0.5 MPa
μ (shear modulus)	20 GPa
V_0 (rigid wall loading rate)	5×10^{-10} m/s
W (rigid wall distance)	100 km

Note. a, b, and σ enter the equations only as $a\sigma$ or $b\sigma$.

direction, where the effective normal stress is a factor of 10 higher. The nearly steady slip within this region encourages more frequent nucleation of SSEs that propagate unilaterally across the fault (Hawthorne & Rubin, 2013b). Relevant parameters are listed in Table 1.

Figure 2a shows an $800L_b$ by $150L_b$ section of the fault, representing the central portion in the strike direction and the full portion in the dip direction. We place circular asperities within a region of dimensions $50L_b$ by $500L_b$ ($0.1W$ by $1W$), representing the tremor zone. We place seven large asperities with a diameter of $30L_b$ separated by $60L_b$ along the fault centerline. Small asperities with a diameter of $8L_b$ are randomly distributed in the tremor zone. Together, the asperities constitute 50% of the area of the tremor zone; the remainder of the tremor zone has the same properties as the background material outside the tremor zone. We subsequently experiment with various combinations of parameters a/b and V_c for the asperities (Figure S4). Although equation (4) is derived for a spring-block-slider system, if we use μ divided by the diameter of the large asperities as a rough estimate of the stiffness k, we find that it also provides a reasonable estimate for the critical value of the slip rate on the background portion of the fault, below which the tremor zone undergoes burst-like behavior. As expected, the small asperities (smaller than $2L_\infty$) are not able to slip much faster than their surroundings due to their large stiffness. It is worth noting that V_c for the asperities is low enough that they do not reach dynamic speeds and should not be viewed as tremor sources. Instead, we view them as simulating the average properties of regions with high tremor source density. We also explore the effect of tidal stresses by adding an external sinusoidal forcing with a period T_{tidal} of about $45D_c/V_c^{bg}$ (12.4 hr for D_c and V_c^{bg} as in Table 1), as shown in Figure S5. The maximum amplitude of tides is set to be $\pm 0.2b^{bg}\sigma$ (1 kPa), comparable to that in Cascadia (Hawthorne & Rubin, 2010). If the ratio of the tidal amplitude to $b^{bg}\sigma$ is higher or the ratio of the tidal period to D_c/V_c^{bg} is higher, the tidal influence is stronger (Hawthorne & Rubin, 2013c).

3.2.2. Results

Figures 2b and 2c show the slip rate evolution along strike during an SSE in one of these simulations. The main front propagation speed within the tremor zone is about 50% faster than that within the background fault. The former is expected to be controlled by the spatial density of the asperities, as well as their a/b and V_c. Beneath southern Vancouver Island, tremor locations from Armbruster et al. (2014) and Peng et al. (2015) suggest that the main front propagation speed is comparable in the updip (high tremor density) and the downdip (low tremor density) areas (see Figure S16 of Peng et al., 2015). Ghosh et al. (2012) inferred a factor of 5 decrease in propagation speed of the main front within areas of high tremor density, but this change in speed seems less obvious in the catalogs of Royer and Bostock (2013) and Peng and Rubin (2016). We find that the propagation speed in our numerical simulations is unrealistically high when the background material to each side of the tremor zone is removed or when the fraction of the area covered by asperities is close to 1. Without tides, each large asperity is capable of rupturing multiple times as the main front passes by, but the interaction among the asperities is complicated (Figure 2b). With tides, many coherent secondary fronts emerge during times of high tidal stress (Figure 2c), most obviously somewhat after the main front has passed, reminiscent of the time-distance plots in Figure 1. As the main front moves through the tremor zone, these secondary

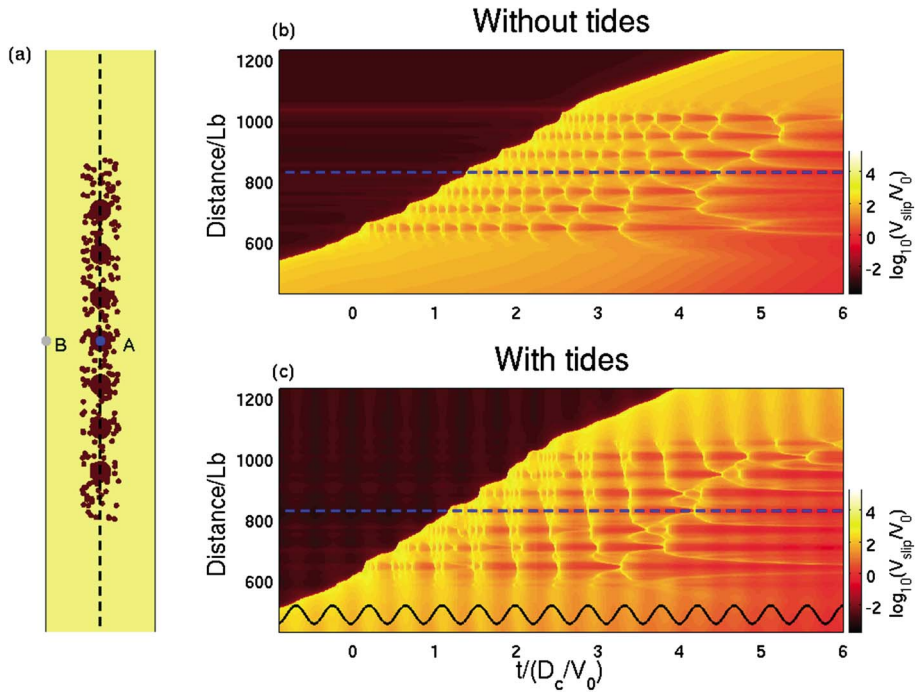

Figure 2. Finite fault simulations with and without tides. (a) The central segment of the fault surface ($800L_b$ along strike and $150L_b$ along dip). The dark red areas are the asperities. Spots A (blue dot) and B (gray dot) are the locations where the slip evolution is shown in Figure 3. (b) and (c) show the slip rate as a function of time along the black-dashed line in (a). The blue-dashed line indicates the spot A. The sinusoidal curve in (c) shows the tidal stress. The *x* and *y* axes are normalized, and values are dimensionless. The parameters *a* and *b* for the asperities are the same as the background. The asperity cutoff velocity V_c^{asp} is 100 times that of the background.

fronts originate from near the main front and propagate backward. Although the recurrence interval is close to the tidal period well behind the front, at the front, it is much shorter, consistent with observations. After the main front moves beyond the end of the tremor zone, several secondary fronts not directly connected to the main front arise. Unlike the observed secondary migrations, however, which propagate at speeds 10–100 times faster than the main front (e.g., Bletery et al., 2017; Ghosh et al., 2010; Houston et al., 2011; Shelly et al., 2007), the secondary fronts in our simulations typically propagate only about 5 times faster than the main front. Snapshots of one of these secondary fronts are shown in Figure S6.

The slip evolution at the center of one of the large asperities is shown in Figure 3. In constrast to the background fault, the asperity sustains multiple bursts with increasing recurrence intervals (Figures 3a and 3b). The profile of the cumulative slip (Figures 3c and 3d) appears to be similar to the observed cumulative event numbers (Figures 1b, 1e, 1h, and 1k). The increase in recurrence interval can also be seen in the interburst times (Figures 3e and 3f). The tidal stress strongly affects the timing of the bursts (Figures 3b, 3d, and 3f), consistent with our observations (Figures 1), as well as with observations of tremor tidal sensitivity after a few days of slip (Houston, 2015), and tidal modulation of RTR occurrence (Thomas et al., 2013).

The total slip during each SSE is roughly $\Delta\tau^{bg}W/\mu$, where W is the distance between the rigid walls ($500L_b$). A dimensional estimate of the stress drop $\Delta\tau^{bg}$ is $(b_{bg}-a_{bg})\sigma\log(V^{bg}_{\tau_{min}}/V_0)$, where $V^{bg}_{\tau_{min}}$ is the slip rate of the minimum steady state stress in the background material. Similarly, the slip accumulated during each burst, D^{asp}, can be approximately estimated to be $\Delta\tau^{asp}L^{asp}/\mu$, where L^{asp} is the diameter of the large asperity and $\Delta\tau^{asp}$ is roughly $(b^{asp}-a^{asp})\sigma\log(V^{asp}_{\tau_{min}}/V_{load})$. We can approximate the loading rate V_{load} from the surrounding slow slip using V_c^{bg}, although we note that V_{load} actually decreases with time, resulting in increasing stress drops for the bursts. Since the backgound fault and the tremor zone accumulate the same amount of slip during an SSE (Figures 3c and 3d), the number of bursts is then D^{bg}/D^{asp}. These rough estimates match the simulation results reasonably well. For example, given the parameters for Figures 3, D^{bg}/D^{asp} is about 16, and we observe 14–15 simulated bursts during an SSE.

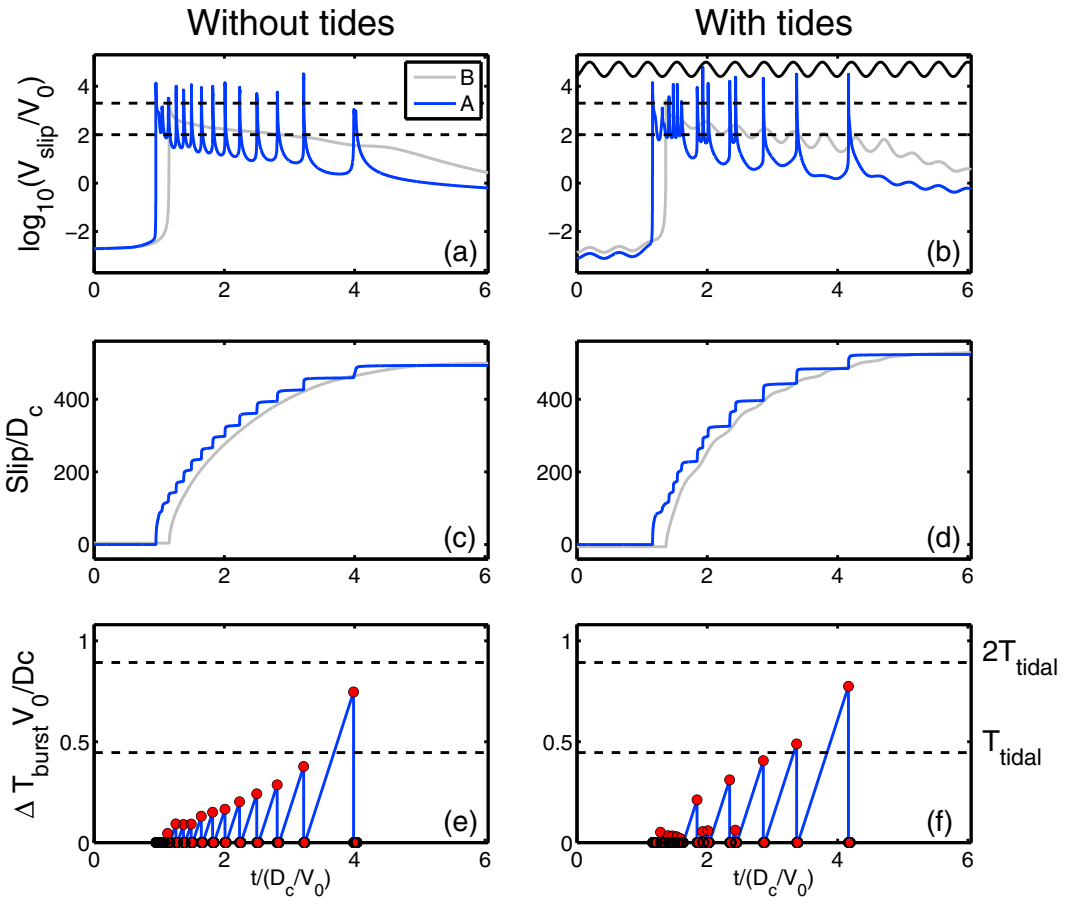

Figure 3. The slip rate (a and b), the cumulative slip (c and d), and the interburst times (e and f) at spots A (blue) and B (gray) in the simulation shown in Figure 2. The second column shows the simulation result with tides (the black sinusoidal curve). Slip starts first at point A because the slow slip front is curved; leading within the tremor zone and lagging outside (Figure S6). The upper-dashed lines in (a) and (b) indicate the critical background slip speed, below which bursts are not expected, inferred using equation (4) and a stiffness of μ divided by the large asperity diameter. The lower-dashed lines indicate the background cutoff velocity V_c^{bg}. The dashed lines in (e) and (f) show the tidal period T_{tidal} and $2T_{tidal}$. The interburst times in (e) and (f) are obtained by assuming that there are observable tremor signals radiated from the asperity at every numerical time step when the slip rate is above V_c^{bg}; choosing other values between this and V^{crit} (the upper-dashed line) does not change the results much. The horizontal and vertical axes in all panels are normalized, and values are dimensionless.

To guard against the possibility that the clustering of interburst times around the tidal period in Figure 3f depends sensitively on the time it takes the main front to propagate the distance between large asperities, we ran a simulation where their spacing is increased from $60L_b$ to $100L_b$. We maintain the asperity fraction at 50%, so the reduced number of large asperities (5 rather than 7) necessitates a larger number of small asperities. We observe behavior similar to that seen in Figures 2 and 3 (Figure S7), which suggests that the separation between large asperities does not significantly influence the time between large bursts in the tidally loaded models.

4. Discussion

The fault heterogeneity in our model, seemingly necessary (in the Earth) for the generation of tremor and probably also the complex tremor migrations behind the main slow slip front, is highly simplified. We do not model individual LFE or tremor sources; rather, the *asperities* that transition to velocity strengthening at a higher sliding speed are intended to represent regions of high LFE density. Although our analytical results for the critical stiffness (equations (3) and (4) are a useful and accurate guide to our numerical simulations, they are derived for asperities with uniform properties, and therefore, there is some ambiguity in interpreting the adopted V_c in terms of natural faults. To give rise to repetitive bursts requires that the sliding speed within

the region of high tremor density be larger than the slip speed averaged over the whole SSE duration. We interpret the V_c within our asperities as reflecting some spatially averaged sliding speed within the region of high low frequency earthquake (LFE) density during tremor bursts, intermediate between the sliding speed on the individual LFE sources and the background material in which those sources are embedded.

Due to the large computational expense, we do not explore tremor zone widths greater than $50L_b$. This width is a few times larger than the nucleation length scale $2L_\infty$ on a strictly velocity weakening fault given the parameters we used (Table 1). The size of the large asperities is chosen such that it is smaller than the tremor zone width and yet large enough that the associated stiffness is small compared to the critical stiffness (equation (3). We have also tested asperity diameters of $20L_b - 40L_b$, which are not shown here, and the results are generally consistent with those shown.

The secondary fronts in our simulations are much slower than those observed in tremor catalogs (e.g., Ghosh et al., 2010; Houston et al., 2011; Shelly et al., 2007). Hawthorne and Rubin (2013c) reported generally less than a factor of 2 increase in propagation speeds for secondary fronts compared to that of the main front on a homogeneous 1-D fault governed by the same friction law as in our study. With the formulation of RSQSim, which adopts several approximations to rate-state friction, Colella et al. (2012) obtained secondary fronts that are on average about 4 times faster than the main front on a 2-D fault. Luo and Ampuero (2014) found that the observed rapid propagation speeds could be reproduced in a model with a velocity-strengthening background and velocity-weakening asperities. A plausible conceptual model could be that numerous velocity-weakening asperities with a spatially varying size distribution are located on the velocity-strengthening fault. Areas with asperities that are mostly small compared to their characteristic nucleation size can generate slow slip accompanied by no or low-density tremor (Skarbek et al., 2012). Areas with large, highly clustered asperities can host repetitive bursts that are driven to failure by the tremor-less slow slip and are able to propagate at speeds one to two orders of magnitude faster than the main front. Another possible explanation for the rapid propagation speeds of the secondary fronts could be that the permeability of the host rock around the fault increases due to slip as the main front moves across the tremor zone, which leads to faster fluid diffusion from the host rock into the shear zone and makes dilatant strengthening of the fault gouge less effective (Peng & Rubin, 2017). This could increase the slip rate and the propagation speed during the secondary fronts.

Despite the low propagation speeds of the secondary fronts, our simple model can reasonably reproduce several key aspects of slow slip evolution, including the similar speeds of the forward-propagating main front within regions with high and low tremor density, the occurrence of repetitive tremor bursts with increasing recurrence intervals, and ultimately tidal modulation. One of the fundamental assumptions of this model is that any region producing repetitive bursts is surrounded by steadier slow slip. In northern Cascadia, there is evidence that slow slip may extend 10–20-km updip of the updip extent of tremor and the along-dip dimension of the slow slip zone, about 60 km (Hall et al., 2018; Houston, 2012; Wech et al., 2009). Many repetitive tremor bursts (including RTRs) appear to occur in the updip portion of the tremorgenic zone (about 20 km), where the tremor density is high (Peng & Rubin, 2016; Peng et al., 2015; Thomas et al., 2013). In Guerrero, the downdip width of the short-term slow slip zone is about 100 km (e.g., Frank et al., 2014, 2015), compared to ~15 km for the minimum dimension (in the strike direction) of the region with repetitive bursts (Figure 1g; Peng & Rubin, 2017). In northern Kii Peninsula, it is not yet clear whether the slow slip zone is larger than the tremor zone or not. High-resolution geodetic data may be needed to resolve this. It is also possible that the regions deficient in tremor, with what we infer to be steadier slip that drives the tremor bursts, do not extend much updip or downdip of localized tremor source regions but are interspersed between them along strike.

Acknowledgments
We thank Satoshi Ide and Suguru Yabe for providing the access to the Hinet seismic data in Japan and Pathikrit Bhattacharya for providing the initial version of the codes to solve the friction equations. Tremor catalogs from Guerrero, Mexico, and northern Kii Peninsula, Japan, are included as supporting information. This research was supported by NSF award EAR-1645145.

References

Ando, R., Nakata, R., & Hori, T. (2010). A slip pulse model with fault heterogeneity for low-frequency earthquakes and tremor along plate interfaces. *Geophysical Research Letters*, *37*, L10310. https://doi.org/10.1029/2010GL043056

Armbruster, J. G., Kim, W., & Rubin, A. M. (2014). Accurate tremor locations from coherent S and P waves. *Journal of Geophysical Research: Solid Earth*, *119*, 5000–5013. https://doi.org/10.1002/2014JB011133

Audet, P., & Kim, Y. (2016). Teleseismic constraints on the geological environment of deep episodic slow earthquakes in subduction zone forearcs: A review. *Tectonophysics*, *670*, 1–15. https://doi.org/10.1016/j.tecto.2016.01.005

Bartlow, N. M., Miyazaki, S., Bradley, A. M., & Segall, P. (2011). Space-time correlation of slip and tremor during the 2009 Cascadia slow slip event. *Geophysical Research Letters*, *38*, L18309. https://doi.org/10.1029/2011GL048714

Beeler, N. M., Tullis, T. E., & Weeks, J. D. (1994). The roles of time and displacement in the evolution effect in rock friction. *Geophysical Research Letters*, *21*, 1987–1990.

Beroza, G. C., & Ide, S. (2011). Slow earthquakes and nonvolcanic tremor. *Annual Review of Earth and Planetary Sciences*, *39*, 271–296.

Bhattacharya, P., Rubin, A. M., Bayart, E. H., Savage, M., & Marone, C. (2015). Critical evaluation of state evolution laws in rate and state friction: Fitting large velocity steps in simulated fault gouge with time-,slip-, and stress-dependent constitutive laws. *Journal of Geophysical Research: Solid Earth*, *120*, 6365–6385. https://doi.org/10.1002/2015JB012437

Bhattacharya, P., Rubin, A. M., & Beeler, N. M. (2017). Does fault strengthening in laboratory rock friction experiments really depend primarily upon time and not slip. *Journal of Geophysical Research: Solid Earth*, *122*, 6389–6430. https://doi.org/10.1002/2017JB013936

Bletery, Q., Thomas, A. M., Hawthorne, J. C., Skarbek, R. M., Rempel, A. W., & Krogstad, R. D. (2017). Characteristics of secondary slip fronts associated with slow earthquakes in Cascadia. *Earth and Planetary Science Letters*, *463*, 212–220.

Bostock, M. G., Thomas, A. M., Savard, G., Chuang, L., & Rubin, A. M. (2015). Magnitudes and moment-duration scaling of low-frequency earthquakes beneath southern Vancouver Island. *Journal of Geophysical Research: Solid Earth*, *120*, 6329–6350. https://doi.org/10.1002/2015JB012195

Colella, H. V., Dieterich, J. H., Richards-Dinger, K., & Rubin, A. M. (2012). Complex characteristics of slow slip events insubduction zones reproduced in multi-cycle simulations. *Geophysical Research Letters*, *39*, L20312. https://doi.org/10.1029/2012GL053276

Dieterich, J. H. (2007). Applications of rate- and state-dependent friction to models of fault slip and earthquake occurrence. In H. Kanamori, & G. Schubert (Eds.), *Treatise on geophysics* (Vol. 4, pp. 6054). Amsterdam: Earthquake Seismology Elsevier.

Dieterich, J. H., & Kilgore, B. D. (1994). Direct observation of frictional contacts: New insights for state-dependent properties. *Pure and Applied Geophysics*, *143*, 283–302.

Dublanchet, P., Bernard, P., & Favreau, P. (2013). Interactions and triggering in a 3-D rate-and-state asperity model. *Journal of Geophysical Research: Solid Earth*, *118*, 2225–2245. https://doi.org/10.1002/jgrb.50187

Fagereng, A., Hillary, G. W. B., & Diener, J. F. A. (2014). Brittle-viscous deformation, slow slip, and tremor. *Geophysical Research Letters*, *41*, 4159–4167. https://doi.org/10.1002/2014GL060433

Frank, WB, Radiguet, M, Rousset, B, Shapiro, NM, Husker, AL, Kostoglodov, V, et al. (2015). Uncovering the geodetic signature of silent slip through repeating earthquakes. *Geophysical Research Letters*, *42*, 2774–2779. https://doi.org/10.1002/2015GL063685

Frank, W. B., Shapiro, N. M., Husker, A. L., Kostoglodov, V., Romanenko, A., & Campillo, M. (2014). Using systematically characterized low-frequency earthquakes as a fault probe in Guerrero, Mexico. *Journal of Geophysical Research: Solid Earth*, *119*, 7686–700. https://doi.org/10.1002/2014JB011457

Ghosh, A., Vidale, J. E., & Creager, K. C. (2012). Tremor asperities in the transition zone control evolution of slow earthquakes. *Journal of Geophysical Research*, *117*, B10301. https://doi.org/10.1029/2012JB009249

Ghosh, A., Vidale, J. E., Sweet, J. R., Creager, K. C., Wech, A. G., Houston, H., et al. (2010). Rapid, continuous streaking of tremor in Cascadia. *Geochemistry, Geophysics, Geosystems*, *11*, Q12010. https://doi.org/10.1029/2010GC003305

Hall, K., Houston, H., & Schmidt, D. A. (2018). Spatial comparisons of tremor and slow slip as a constraint on fault strength in the northern Cascadia subduction zone. *Geochemistry, Geophysics, Geosystems*, *19*. https://doi.org/10.1029/2018GC007694

Hawthorne, J. C., Bostock, M. G., Royer, A. A., & Thomas, A. M. (2016). Variations in slow slip moment rate associated with rapid tremor reversals in Cascadia. *Geochemistry, Geophysics, Geosystems*, *17*, 4899–919. https://doi.org/10.1002/2016GC006489

Hawthorne, J. C., & Rubin, A. M. (2010). Tidal modulation of slow slip in Cascadia. *Journal of Geophysical Research*, *115*, B09406. https://doi.org/10.1029/02010JB007502

Hawthorne, J. C., & Rubin, A. M. (2013a). Short time scale correlation between slow slip and tremor in Cascadia. *Journal of Geophysical Research: Solid Earth*, *118*, 1316–1329. https://doi.org/10.1002/jgrb.50103

Hawthorne, J. C., & Rubin, A. M. (2013b). Laterally propagating slow slip events in a rate and state friction model with a velocity-weakening to velocity-strengthening transition. *Journal of Geophysical Research: Solid Earth*, *118*, 3785–3808. https://doi.org/10.1002/jgrb.50261

Hawthorne, J. C., & Rubin, A. M. (2013c). Tidal modulation and back-propagating fronts in slow slip events simulated with a velocity-weakening to velocity-strengthening friction law. *Journal of Geophysical Research: Solid Earth*, *118*, 1216–1239. https://doi.org/10.1002/jgrb.50107

Hirose, H., & Obara, K. (2005). Repeating short- and long-term slow slip events with deep tremor activity around the Bungo channel region, southwest Japan. *Earth Planets Space*, *57*(10), 961–972.

Hirose, H., & Obara, K. (2006). Short-term slow slip and correlated tremor episodes in the Tokai region, central Japan. *Geophysical Research Letters*, *33*, L17311. https://doi.org/10.1029/2006GL026579

Horowitz, F. G., & Ruina, A. (1989). Slip patterns in a spatially homogeneous fault model. *Journal of Geophysical Research (19782012)*, *94*(B8), 10279–10298.

Houston, H. (2012). *Slow slip may extend updip of tremor in Northern Cascadia ETSs*. Abstract S42B-06 presented at 2012 Fall Meeting AGU. San Francisco, CA.

Houston, H. (2015). Low friction and fault weakening revealed by rising sensitivity of tremor to tidal stress. *Nature Geoscience*, *8*, 409–415. https://doi.org/10.1038/ngeo2419

Houston, H., Delbridge, B. G., Wech, A. G., & Creager, K. C. (2011). Rapid tremor reversals in Cascadia generated by a weakened plate interface. *Nature Geoscience*, *4*(6), 404–409. https://doi.org/10.1038/ngeo1157

Ide, S. (2010). Striations, duration, migration and tidal response in deep tremor. *Nature*, *466*, 356–359. https://doi.org/10.1038/nature09251

Liu, Y. J., & Rice, J. R. (2005). Aseismic slip transients emerge spontaneously in three-dimensional rate and state modeling of sub- duction earthquake sequences. *Journal of Geophysical Research*, *110*, B08307. https://doi.org/10.1029/2004JB003424

Liu, Y., & Rice, J. R. (2007). Spontaneous and triggered aseismic deformation transients in a subduction fault model. *Journal of Geophysical Research*, *112*, B09404. https://doi.org/10.1029/2007JB004930

Liu, Y., & Rubin, A. M. (2010). Role of fault gouge dilatancy on aseismic deformation transients. *Journal of Geophysical Research*, *115*, B10414. https://doi.org/10.1029/2010JB007522

Luo, Y., & Ampuero, J.-P. (2014). A model of spontaneous complex tremor migration patterns and background slow-slip events via interaction of brittle asperities and a ductile matrix. AGU, Fall meeting 2014, abstract S52B-01.

Obara, K. (2002). Nonvolcanic deep tremor associated with subduction in southwest Japan. *Science*, *296*(5573), 1679–1681. https://doi.org/10.1126/science.1070378

Obara, K. (2010). Phenomenology of deep slow earthquake family in southwest Japan: Spatiotemporal characteristics and segmentation. *Journal of Geophysical Research*, *115*, B00A25. https://doi.org/10.1029/2008JB006048

Obara, K., & Hirose, H. (2006). Non-volcanic deep low-frequency tremors accompanying slow slips in the southwest Japan subduction zone. *Tectonophsyics*, *417*, 33–51.

Obara, K., Hirose, H., Yamamizu, F., & Kasahara, K. (2004). Episodic slow slip events accompanied by non-volcanic tremors in southwest Japan subduction zone. *Geophysical Research Letters*, *31*, L23602. https://doi.org/10.1029/2004GL020848

Peng, Y., & Rubin, A. M. (2016). High-resolution images of tremor migrations beneath the Olympic Peninsula from stacked array of arrays seismic data. *Geochemistry, Geophysics, Geosystems*, *17*, 587–601. https://doi.org/10.1002/2015GC006141

Peng, Y., & Rubin, A. M. (2017). Intermittent tremor migrations beneath Guerrero, Mexico, and implications for fault healing within the slow slip zone. *Geophysical Research Letters*, *44*, 760–770. https://doi.org/10.1002/2016GL071614

Peng, Y., Rubin, A. M., Bostock, M. G., & Armbruster, J. G. (2015). High-resolution imaging of rapid tremor migrations beneath southern Vancouver Island using cross-station cross correlations. *Journal of Geophysical Research: Solid Earth*, *120*, 4317–4332. https://doi.org/10.1002/2015JB011892

Radiguet, M., Cotton, F., Vergnolle, M., Campillo, M., Valette, B., Kostoglodov, V., et al. (2011). Spatial and temporal evolution of a long term slow slip event: The 2006 Guerrero slow slip event. *Geophysical Journal International*, *184*(2), 816–828. https://doi.org/10.1111/j.1365-246X.2010.04866.x

Rice, J. R., & Ruina, A. L. (1983). Stability of steady frictional slipping. *Journal of Applied Mechanics*, *50*, 343–349.

Rogers, G., & Dragert, H. (2003). Episodic tremor and slip on the Cascadia subduction zone: The chatter of silent slip. *Science*, *300*(5627), 1942–1943. https://doi.org/10.1126/science.1084783

Royer, A. A., & Bostock, M. G. (2013). A comparative study of low frequency earthquake templates in northern Cascadia. *Earth and Planetary Science Letters*, *1*(5627), 1–10. https://doi.org/10.1016/j.epsl.2013.08.040

Royer, A., Thomas, A. M., & Bostock, M. G. (2014). Tidal modulation and triggering of low-frequency earthquakes in northern Cascadia. *Journal of Geophysical Research: Solid Earth*, *120*, 384–405. https://doi.org/10.1002/2014JB011430

Rubin, A. M., & Ampuero, J.-P. (2005). Earthquake nucleation on (aging) rate and state faults. *Journal of Geophysical Research*, *110*, B11312. https://doi.org/10.1029/2005JB003686

Rubin, A. M., & Armbruster, J. G. (2013). Imaging slow slip fronts in Cascadia with high precision cross-station tremor locations. *Geochemistry, Geophysics, Geosystems*, *14*, 12. https://doi.org/10.1002/2013GC005031

Ruina, A. (1983). Slip instability and state variable friction laws. *Journal of Geophysical Research*, *88*(B12), 10,359–10,370. https://doi.org/10.1029/JB088iB12p10359

Schwartz, S. Y., & Rokosky, J. M. (2007). Slow slip events and seismic tremor at circum-Pacific subduction zones. *Reviews of Geophysics*, *45*, RG3004. https://doi.org/10.1029/2006RG000208

Segall, P., Rubin, A. M., Bradley, A. M., & Rice, J. R. (2010). Dilatant strengthening as a mechanism for slow slip events. *Journal of Geophysical Research*, *115*, B12305. https://doi.org/10.1029/2010JB007449

Shelly, D. R., Beroza, G. C., & Ide, S. (2007). The complex evolution of transient slip derived from precise tremor locations in western Shikoku, Japan. *Geochemistry, Geophysics, Geosystems*, *8*, Q10014. https://doi.org/10.1029/2007GC001640

Shelly, D. R., Beroza, G. C., Ide, S., & Nakamula, S. (2006). Low-frequency earthquakes in Shikoku, Japan, and their relationship to episodic tremor and slip. *Nature*, *442*(7099), 188–191.

Shibazaki, B., & Iio, Y. (2003). On the physical mechanism of silent slip events along the deeper part of the seismogenic zone. *Geophysical Research Letters*, *30*(9), 1489. https://doi.org/10.1029/2003GL017047

Shibazaki, B., & Shimamoto, T. (2007). Modelling of short-interval silent slip events in deeper subduction interfaces considering the frictional properties at the unstable stable transition regime. *Geophysical Journal International*, *171*(1), 191–205. https://doi.org/10.1111/j.1365-790 246X.2007.03434.x

Skarbek, R. M., Rempel, A. W., & Schmidt, D. A. (2012). Geologic heterogeneity can produce aseismic slip transients. *Geophysical Research Letters*, *39*, L21306. https://doi.org/10.1029/2012GL053762

Suzuki, T., & Yamashita, T. (2009). Dynamic modeling of slow earthquakes based on thermoporoelastic effects and inelastic generation of pores. *Journal of Geophysical Research*, *114*, B00A04. https://doi.org/10.1029/2008JB006042

Sweet, J. R., Creager, K. C., Thomas, T., Vidale, J. E., & Houston, H. (2012). *Unlocking the secrets of slow slip on the plate interface using Cascadia LFEs*. Abstract S43I-04 presented at 2012 Fall Meeting AGU. San Francisco, CA.

Thomas, T. W., Vidale, J. E., Houston, H., Creager, K. C., Sweet, J. R., & Ghosh, A. (2013). Evidence for tidal triggering of high-amplitude rapid tremor reversals and tremor streaks in northern Cascadia. *Geophysical Research Letters*, *40*, 4254–4259. https://doi.org/10.1002/grl.50832

Wech, A. G., Creager, K. C., & Melbourne, T. I. (2009). Seismic and geodetic constraints on Cascadia slow slip. *Journal of Geophysical Research*, *114*, B10316. https://doi.org/10.1029/2008JB006090